

Shot interpolation for radon multiple suppression

Sean Crawley¹

keywords: *missing data, interpolation*

ABSTRACT

Decreased CMP fold, such as that found in multi-source, multi-streamer acquisition geometries, can hinder processing steps which benefit from well sampled CMP gathers, such as radon transforms. In two steps of linear least squares, multiscale prediction-error filters (PEF)s can estimate local dips from the recorded data and then use the dip information to fill in unrecorded shot or receiver gathers. In this paper I use multiscale, volumetric PEFs to interpolate sparse, multiple-contaminated data. The increase in fold improves multiple-suppression results.

INTRODUCTION

In multi-source acquisition, the normal spatial undersampling of CMP gathers is compounded by the fact that at each inline source location, only one of the sources is fired. This allows acquisition, which is expensive, to go more quickly, but reduces sampling at a given midpoint to every fourth offset (in the case of two sources), which may cause problems for later processing steps, such as radon multiple suppression (Marfurt et al., 1996).

In this paper I subsample a multiple-contaminated 2-D marine synthetic survey to simulate a single inline from a multi-source survey. The degraded sampling hampers radon multiple attenuation. In a sequence of two steps of linear least squares, I estimate a set of local multiscale PEFs and re-estimate the removed traces. This is similar to a time-domain implementation of Spitz's algorithm (1991), with the benefit of control over the effective filter length in time (Abma and Claerbout, 1995). Infilling the removed data improves the separation of multiple and primary energy in radon transform space.

¹**email:** sean@sep.stanford.edu

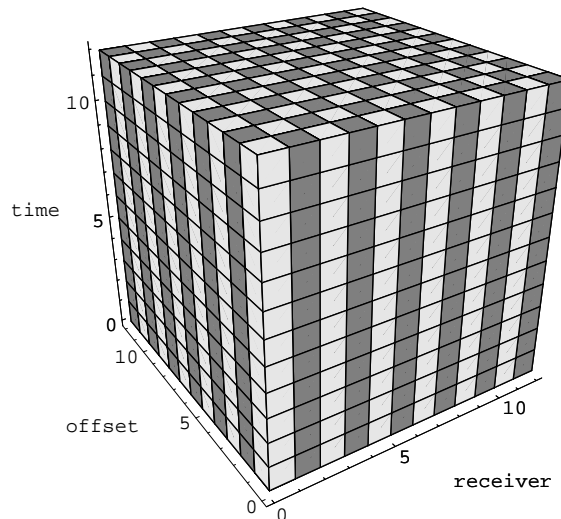
ESTIMATING MISSING DATA

Multi-Scale Filters

Missing data is estimated in two steps of linear least squares (Claerbout, 1992). The first step is estimation of PEFs. Prediction-error filters are good at estimating lines or planes of constant dip, but not curves. Individual filters are estimated on small patches so events appear as dipping planes of approximately constant dip.

The shape of a 3-D PEF with five points on the time axis, and three and two points respectively on two space axes is shown in Figure 3. The dark shaded box is constrained to hold the value 1, the light boxes are adjustable coefficients. The filter forms a half volume, which can be oriented in different ways. To find the values of the adjustable coefficients, specify that the convolution of the filter with the known data gives the minimum power. This means solving the regression $0 \approx \mathbf{Y}\mathbf{a}$, where \mathbf{a} is a vector containing the filter and \mathbf{Y} is convolution with the recorded data. Constraining one filter coefficient to 1 (the shaded box in Figure 3) prevents the trivial answer $\mathbf{a} = 0$.

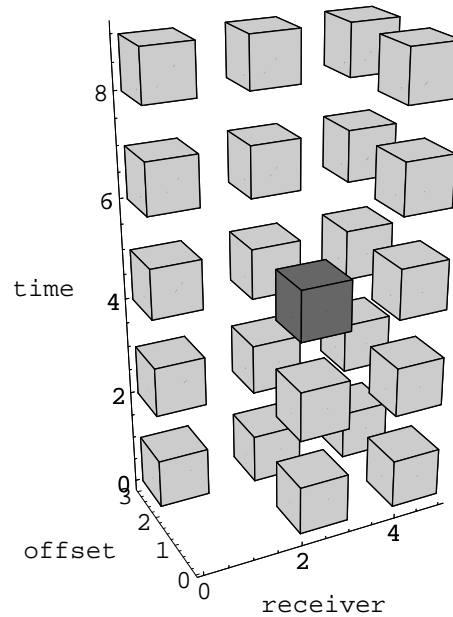
Figure 1: Representation of input data cube. Recorded traces are dark, traces to be interpolated are light. `sean1-dataPic` [NR]



The data are sorted so the recorded traces and the traces to be interpolated are arranged in the input cube in a checkerboard pattern. In the case of missing shots (or dual-source marine geometry), this corresponds to a cube with time, receiver location, and offset coordinates. For comparison with the filter shapes, the input cube is represented by Figure 1, with the shaded squares corresponding to empty trace bins. The checkerboard arrangement has the intuitively pleasing quality that every missing trace is surrounded on four sides by a recorded trace. It also poses the problem that there is no densely sampled patch for estimating a filter such as the one in Figure 3. Any regression equations that have zeroes in them should be dropped.

For the filter shown in Figure 3, this eliminates all the regression equations. To make the filter estimation work, we scale all the axes of the filter by two. This gives the expanded filter shown in Figure 2. Convolved across a checkerboard of present and missing data, this filter alternately hits exclusively filled and exclusively empty bins. Because all the axes are scaled equally, the expanded and compressed filters are self-similar and have the same dip information (Claerbout, 1992).

Figure 2: Representation of expanded PEF. Dark square is constrained to be a 1. Light squares are coefficients adjusted to minimize output power when convolved with grid of Figure 1.
sean1-expandedAltBW [NR]

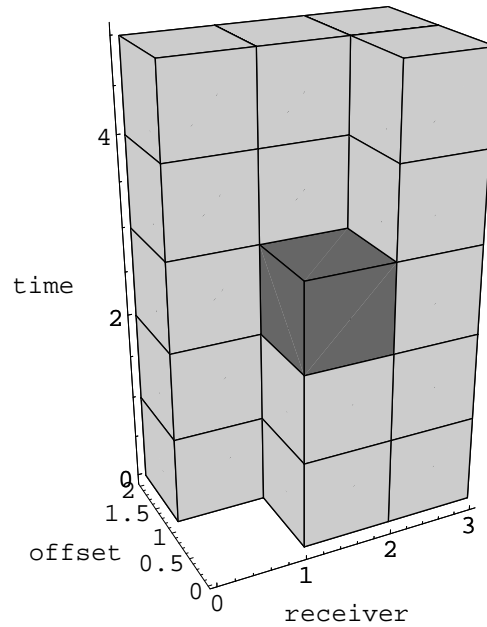


After the filter has been estimated it is used to fill in the empty trace bins. This is the second step of least squares. We want the recorded and estimated data to have the same dips. Since the dip information is now carried in the PEF, this is once again specifying that the convolution of the filter and data should give the minimum output, except that now the filter is known and the data is unknown. We constrain the data by specifying that the originally recorded data cannot change. To separate the known and unknown data we have a known data selector \mathbf{K} and an unknown data selector \mathbf{U} , with $\mathbf{U} + \mathbf{K} = \mathbf{I}$. These multiply by 1 or 0 depending on whether the data was originally recorded or not. With \mathbf{A} signaling convolution with the PEF and \mathbf{y} the vector of data, the regression is $0 \approx \mathbf{A}(\mathbf{U} + \mathbf{K})\mathbf{y}$, or $\mathbf{A}\mathbf{U}\mathbf{y} \approx -\mathbf{A}\mathbf{K}\mathbf{y}$. To fill the missing bins, the filter must touch both filled and empty bins together, so it gets compressed to look like Figure 3.

Example

The data in this test is intended to represent a single inline from a dual-source, multi-streamer data set, where each individual source's shot interval is twice the receiver

Figure 3: Representation of PEF. Coefficients are same as Figure 2. This filter is applied to grid of Figure 1 to find missing traces. `sean1-notExpandedAltBW` [NR]



interval. One source is typically fired for each receiver interval that the boat travels, with the sources alternating. A given CMP gather in this case contains only every fourth recorded offset. The data are reinterpolated to the original sampling, where the intervals are equal, doubling the data.

Results sorted into an example CMP gather and windowed are shown in Figures 4. The left side shows the original data, the center shows the output after throwing out every other offset and interpolating with local volume prediction error filters, and the right side shows the residual clipped for comparison. Figure 4 is a window from the near offset traces. Here the data have noticeable curvature, and so they are difficult to predict and there is some energy in the residual. Happily, energetic events are reconstructed with good fidelity. At farther offsets (not shown), where events tend to become much more linear, the residual vanishes completely.

Because the motivation for resampling in this case is multiple suppression, Figure 5 shows portions of parabolic radon transforms for these same data. In these figures the left shows the radon transform of the original data, the center shows the transform of the decimated data, and the right shows the transform of the reinterpolated data. The center panel shows that the primaries in the decimated data are poorly represented in the radon transform, especially in the complex area around 2.5 to 3.7 seconds. The decimated data also shows more artifact energy in the multiple region of the transform. The original and interpolated data produce better radon transforms.

CMP gathers after radon demultiple are shown in Figure 6. The left panel shows a portion of a CMP gather with alternate offsets removed and radon demultiple applied.

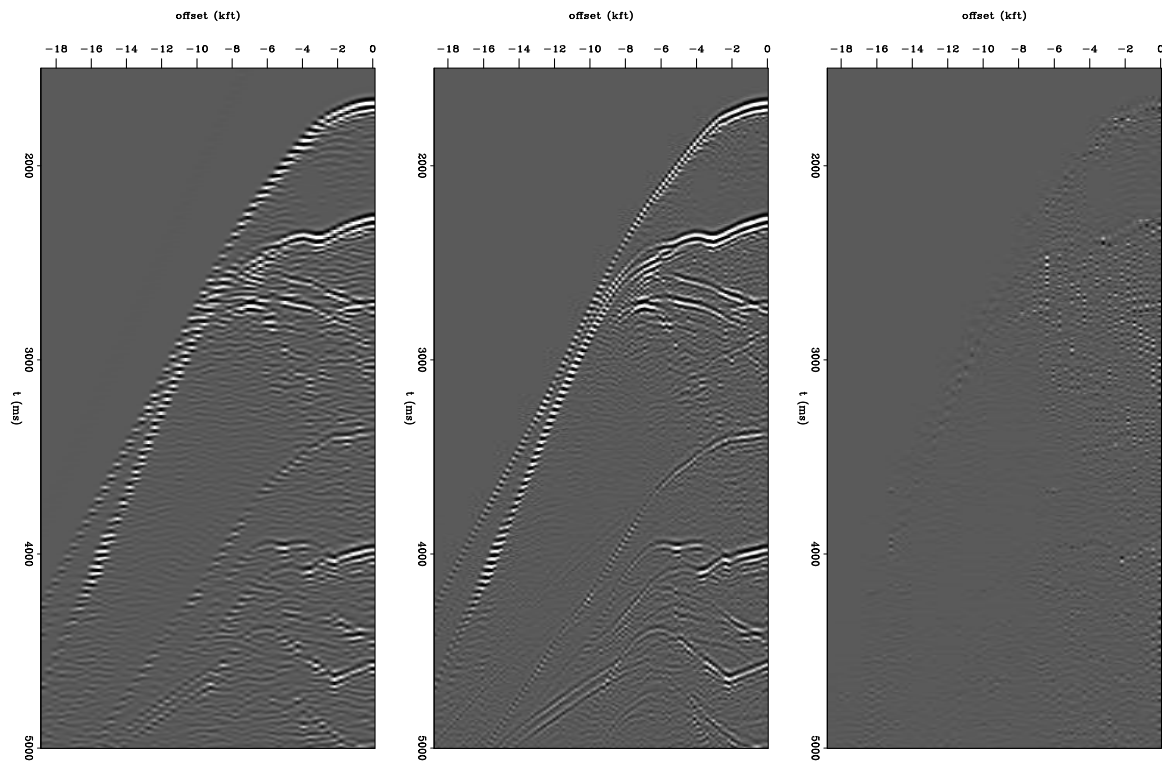


Figure 4: Near offset window from CMP gather. Left side shows decimated data volume. Center shows output after reinterpolation. Right side shows residual clipped to match. `sean1-compWin0` [CR]

The right panel shows the same portion with the removed offsets reinterpolated, radon demultiple applied, and the interpolated traces thrown away. The left panel shows less suppression of various multiple events, most notably the steep multiples labeled **A**, and also some attenuation of primary energy, such as at **B**.

Figure 7 shows a subsalt portion of a stacked section. The left panel shows the result of radon demultiple and stack on the decimated data, the right panel shows the result of simple stack on the interpolated data. The reason for the difference in flow is that simply stacking the data which has been dealiased by interpolation (leaving out the innermost few traces) removes most of the multiple energy, but doing a similar operation on the decimated data (left panel) gives a terrible result, because the aliased nature of the multiples causes them to come through in the stack as a short-period (50ms or so) series of seafloor multiples that completely obscures the section. At any rate, the right panel is approximately identical with or without going to the trouble of radon transform. Strong multiple events (examples at **A**) are suppressed more or less equivalently in the two sections; arguably somewhat better in the interpolated data. Some important primaries at **B** are significantly attenuated in the decimated data, as shown by comparison with the interpolated data. Also, throughout the section, most visible in the neighborhood of **C**, aliasing results in layer-like artifacts. Finally, many interesting arrivals, especially diffractions, in the faulted area around **D** are strongly attenuated in the decimated data.

CONCLUSIONS

The results are very satisfying. Naturally an unaliased wavefield is preferable to an aliased wavefield, if the data are interpolated with good fidelity. The interpolation residual is non-zero but mostly small, especially at far offsets. The example presented in this abstract is a 2-D survey, the theory is unchanged in 3-D, and fidelity will probably be better, thanks to the added directions of prediction.

ACKNOWLEDGEMENTS

The data, and some enlightening email, were provided by Scott Michell of BP.

REFERENCES

- Abma, R., and Claerbout, J., 1995, Lateral prediction for noise attenuation by t-x and f-x techniques: *Geophysics*, **60**, no. 6, 1887–1896.
- Claerbout, J. F., 1992, *Earth Soundings Analysis: Processing Versus Inversion*: Blackwell Scientific Publications.

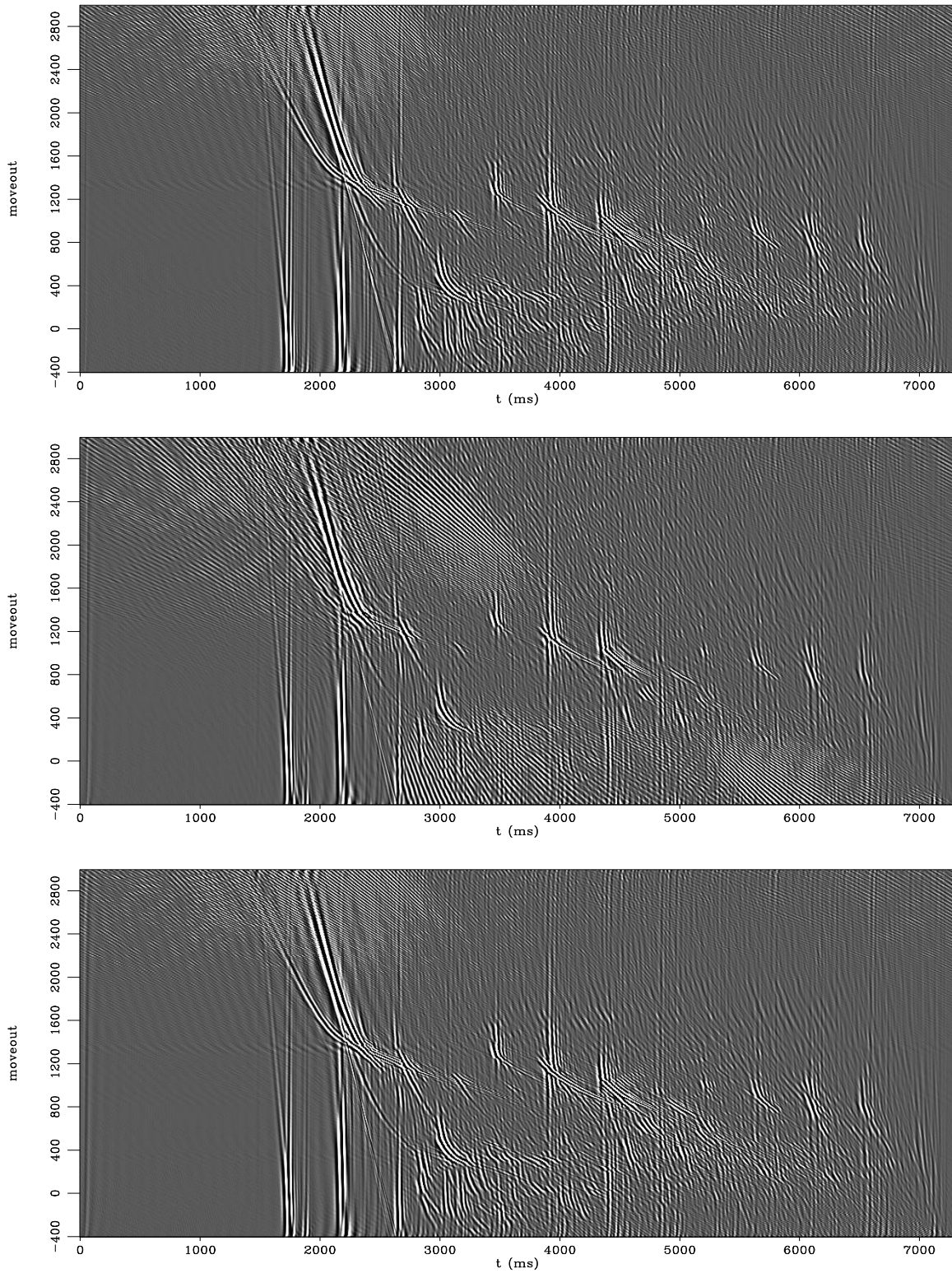


Figure 5: Windows from radon transforms. Left side (bottom) shows radon transform of original CMP gather. Center shows transform of decimated CMP gather. Right (top) shows transform of reinterpolated data. Note decimated gather (center panel) generated many more aliasing-related artifacts and poor representation of primaries. [sean1-cr90](#) [CR]

Marfurt, K. J., Schneider, R. V., and Mueller, M. C., 1996, Pitfalls of using conventional and discrete radon transforms on poorly sampled data: *Geophysics*, **61**, no. 5, 1467–1488.

Spitz, S., 1991, Seismic trace interpolation in the f-x domain: *Geophysics*, **56**, no. 6, 785–794.

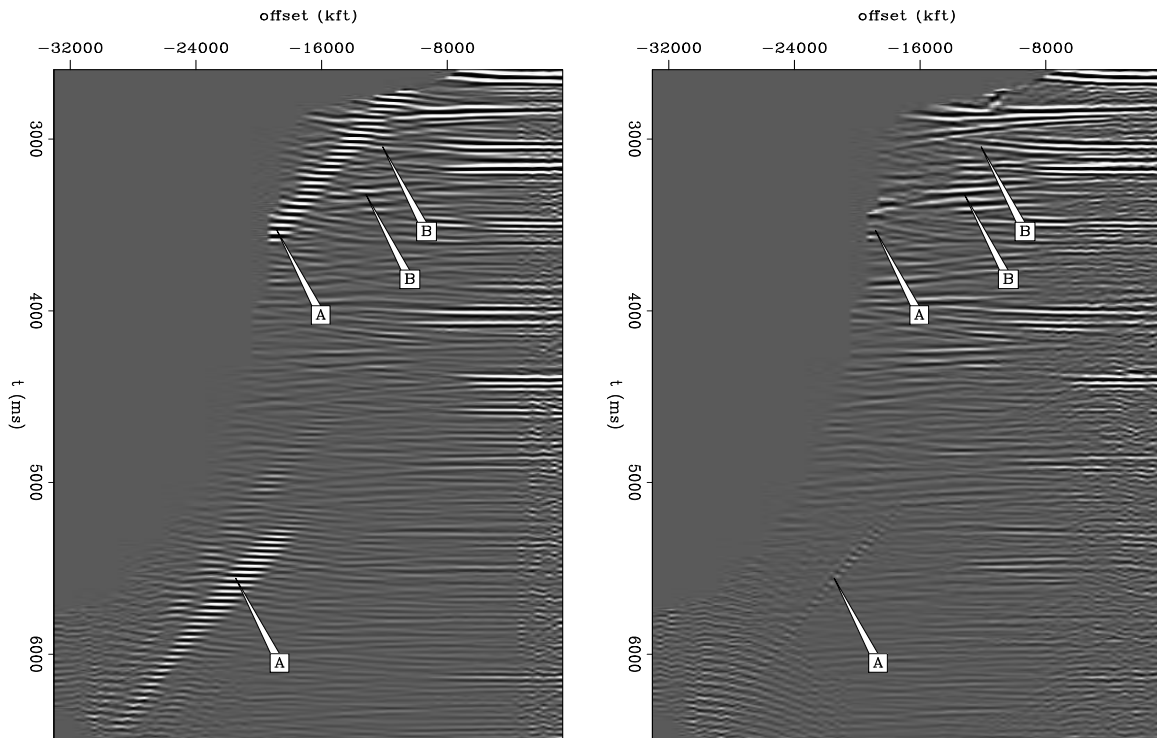


Figure 6: Portions of CMP gathers after radon demultiple. Left shows decimated CMP gather. Right side shows reinterpolated CMP gather, with interpolated traces thrown out after radon demultiple. Note that in the left panel aliased multiples at far offset are not well suppressed (**A**), and that some interesting energy in the mostly primary region around 3 seconds is attenuated (**B**). `sean1-compCmp` [CR]

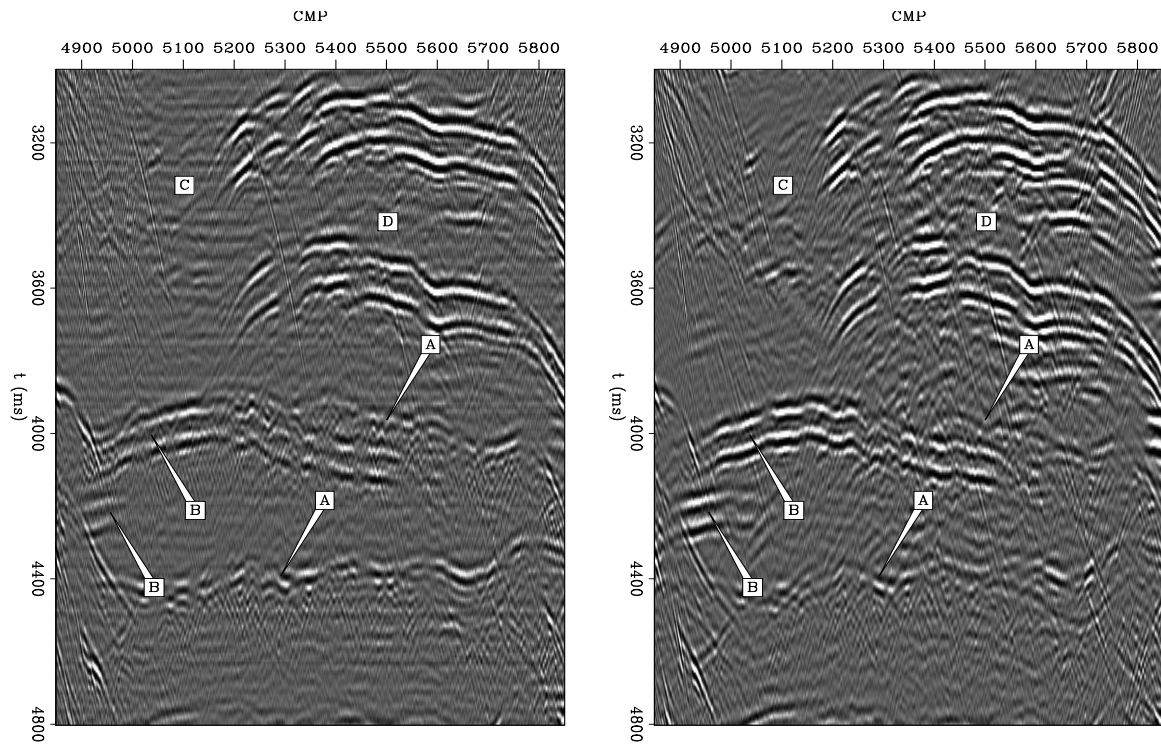


Figure 7: Subsalt portion of stacked section. The left panel shows decimated data after demultiple and stack, the right panel shows same data after interpolation and stack. Multiples (**A**) are arguably better attenuated in the interpolated data. The decimated data shows attenuated primary events (**B**), and layer-like artifacts (**C**). `sean1-compStack` [CR]